

Observation of an isotropic superconducting gap at the Brillouin zone centre of $\text{Tl}_{0.63}\text{K}_{0.37}\text{Fe}_{1.78}\text{Se}_2$

X.-P. WANG^{1,2}, P. RICHARD^{1(a)}, X. SHI¹, A. ROEKEGHEM^{1,3}, Y.-B. HUANG¹, E. RAZZOLI², T. QIAN¹, E. RIENKS⁴, S. THIRUPATHAIAH⁴, H.-D. WANG⁵, C.-H. DONG⁵, M.-H. FANG⁵, M. SHI² and H. DING^{1(b)}

¹ *Beijing National Laboratory for Condensed Matter Physics, and Institute of Physics, Chinese Academy of Sciences Beijing 100190, China*

² *Paul Scherrer Institut, Swiss Light Source - CH-5232 Villigen PSI, Switzerland*

³ *Centre de Physique Théorique, Ecole Polytechnique, CNRS - F-91128 Palaiseau Cedex, France, EU*

⁴ *Helmholtz-Zentrum Berlin, BESSY - D-12489 Berlin, Germany, EU*

⁵ *Department of Physics, Zhejiang University - Hangzhou 310027, China*

received on 27 August 2012; accepted by J. Fink on 27 August 2012

published online 12 September 2012

PACS 74.70.Xa – Pnictides and chalcogenides

PACS 74.25.Jb – Electronic structure (photoemission, etc.)

PACS 79.60.-i – Photoemission and photoelectron spectra

Abstract – We performed a high-resolution angle-resolved photoemission spectroscopy study on superconducting (SC) $\text{Tl}_{0.63}\text{K}_{0.37}\text{Fe}_{1.78}\text{Se}_2$ ($T_c = 29$ K) in the whole Brillouin zone (BZ). In addition to a nearly isotropic ~ 8.2 meV 2-dimensional (2D) SC gap ($2\Delta/k_B T_c \sim 7$) on quasi-2D electron Fermi surfaces (FSs) located around $M(\pi, 0, 0)$ - $A(\pi, 0, \pi)$, we observe a ~ 6.2 meV isotropic SC gap ($2\Delta/k_B T_c \sim 5$) on the Z -centred electron FS that rules out any d -wave pairing symmetry and rather favors an s -wave symmetry. All isotropic SC gap amplitudes can be fit by a single-gap function derived from a local strong-coupling approach suggesting an enhancement of the next-nearest neighbor exchange interaction in the ferrochalcogenide superconductors.

Copyright © EPLA, 2012

One of the most important and intensively debated issues in Fe-based superconductivity is whether the superconducting (SC) pairing is caused by itinerant magnetic fluctuations enhanced by Fermi surface (FS) quasi-nesting or by local magnetic superexchange interactions [1]. For most Fe-based superconductors, which have quasi-nested hole and electron FSs separated by the antiferromagnetic (AF) vector, both the weak-coupling itinerant and the strong-coupling local approaches predict a similar sign-reversed s -wave pairing symmetry. However, for the newly discovered ferrochalcogenide superconductor $\text{A}_x\text{Fe}_2\text{Se}_2$ ($A = \text{K}, \text{Rb}, \text{Cs}, \text{Tl}$) [2,3], which does not have hole FS pocket at the Brillouin zone (BZ) centre as observed by angle-resolved photoemission spectroscopy (ARPES) [4–7], most calculations [8–13] based on the weak-coupling approach predict a sign reversal in the gap between the electron FS sheets located at $M(\pi, 0)$ and $\bar{M}(0, \pi)$ (here defined in the 1 Fe/unit cell notation) naturally described by a d -wave symmetry. On the other

hand, the strong-coupling approach still favors a s -wave symmetry [14–16,16–19].

Although the observation by ARPES of an isotropic SC gap on the electron FSs at the zone boundary [4–6] supports the s -wave scenario, it cannot completely rule out a d -wave symmetry which in principle can be nodeless if the nodal lines do not intersect any FS. Luckily, there is a 3-dimensional (3D) electron FS pocket centred around $Z(0, 0, \pi)$ as previously reported by ARPES [5,20], which can be used to distinguish d -wave from s -wave symmetry since the d -wave symmetry would create nodes along a pair of perpendicular directions on this FS pocket [11–13]. Therefore, the momentum (k)-dependence of the SC gap on this electron FS is crucial in determining the pairing symmetry and mechanism of this superconductor and possibly the entire family of Fe-based superconductors.

In this letter, we report high-resolution ARPES measurements on SC $\text{Tl}_{0.63}\text{K}_{0.37}\text{Fe}_{1.78}\text{Se}_2$ ($T_c = 29$ K) in the whole 3D BZ by tuning the incident photon energy. We observe a nearly isotropic and nearly k_z -invariant ~ 8.2 meV SC gap on electron FS pockets located around M , in agreement with our previous report on the same

^(a)E-mail: p.richard@iphy.ac.cn

^(b)E-mail: dingh@iphy.ac.cn

material using a He discharge lamp [4]. More significantly, a nearly isotropic SC gap with a smaller size of ~ 6.2 meV is observed on the 3D electron FS pocket around Z , without obvious variation along k_z . This smaller gap closes at the same temperature as the larger gap near M [4], suggesting a same pairing channel for the two different FSs. Our observation of a nodeless SC gap structure for the whole k -space rules out the d -wave pairing and rather supports a s -wave symmetry. Interestingly, the global gap structure in this material can be described by a single-gap function derived from a strong-coupling approach [15,16].

High-quality single crystals of $\text{Tl}_{0.63}\text{K}_{0.37}\text{Fe}_{1.78}\text{Se}_2$ ($T_c^{\text{onset}} = 29.1$ K; $T_c^{\text{mid}} = 28.6$ K; $T_c^{\text{zero}} = 27.5$ K) were grown by the Bridgeman method [3]. The precise composition was determined using energy dispersive X-ray spectrometry (EDXS). The lattice parameters $a = 3.85$ Å and $c = 14.05$ Å were determined by fitting XRD data. ARPES measurements were performed at the 1-cubed ARPES end-station of BESSY and at Swiss Light Source beamline SIS using a VG-Scienta R4000 electron analyzer with photon energy ranging from 18 to 63 eV. The angular resolution was set to 0.2° and the energy resolution to 5–7 meV for SC gap measurements at $T = 0.9$ K. The band structure and temperature-dependent SC gap sizes were recorded with 10–15 meV energy resolution. All samples were cleaved *in situ* and measured in a working vacuum better than 5×10^{-11} torr. For convenience, we describe all the results using the 1 Fe site/unit cell (or unfolded) notation and use $c' = c/2 = 7.025$ Å. In the following, we also use $\bar{\Gamma}$ and \bar{M} to refer to any point along the $\Gamma(0, 0, 0)$ - $Z(0, 0, \pi)$ axis and $M(0, \pi, 0)$ - $A(0, \pi, \pi)$ axis, respectively.

In fig. 1(a), we show an ARPES FS intensity mapping of $\text{Tl}_{0.63}\text{K}_{0.37}\text{Fe}_{1.78}\text{Se}_2$ recorded in the normal state (35 K) with 63 eV photons. As with previous results [4–7,20], the dominant feature is an almost circular electron FS centred at the \bar{M} -point. An additional weak-intensity spot is also detected at $\bar{\Gamma}$. We display in figs. 1(b) and (c) the ARPES cuts recorded along $\bar{\Gamma}$ - \bar{M} with p -polarized and s -polarized light, respectively. As with the corresponding sets of energy distribution curves (EDCs) given in figs. 1(d) and (e), they indicate that this feature has an electron-like dispersion that will hereafter be called the κ band. In agreement with a previous study on $(\text{Tl,Rb})_y\text{Fe}_{2-x}\text{Se}_2$ [20], our light polarization analysis indicates that the κ band is enhanced with p polarization as compared with s polarization.

The out-of-plane momentum k_z can be approximated in ARPES experiments by tuning the photon energy over a wide range. The estimated values of k_z are given by $k_z = \sqrt{2m_e/\hbar^2[(\hbar\nu - \phi - E_B)\cos^2\theta + V_0]}$, where ϕ is the work function, V_0 is the inner potential of the sample (estimated to 12 eV for this material from the periodic dispersion along k_z), and θ is the emission angle [21]. In fig. 1(f), we show the intensity mapping in the k_x - k_z plane of $\text{Tl}_{0.63}\text{K}_{0.37}\text{Fe}_{1.78}\text{Se}_2$ over one half-cycle. According to our analysis, $\hbar\nu = 18$ and 30 eV are close to the $\bar{\Gamma}$ and Z

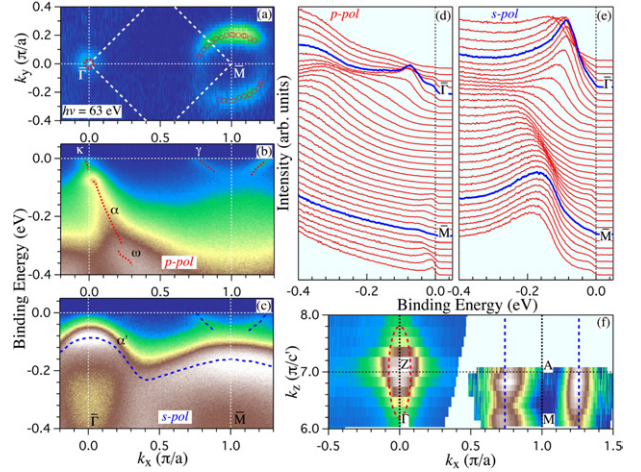


Fig. 1: (Colour on-line) (a) ARPES FS intensity map of $\text{Tl}_{0.63}\text{K}_{0.37}\text{Fe}_{1.78}\text{Se}_2$ (± 5 meV integrated window) recorded in the normal state (35 K) with 63 eV photons. Open circles and filled triangles correspond to k_F locations of the γ and κ bands, respectively. (b) ARPES intensity plot ($\hbar\nu = 63$ eV) for a cut along the $\bar{\Gamma}$ - \bar{M} direction recorded at 35 K with a p polarization. Guides to the eye are plotted for the various bands observed. (c) Same as (b) but using s -polarized photons. (d), (e) EDCs corresponding to the cuts in (b) and (c), respectively. (f) ARPES intensity plot in the k_z - k_x plane. The red and blue dashed lines indicate the k_F locations.

points, respectively. While the FS centred at \bar{M} does not disperse with k_z , strong k_z modulations are observed for the small 3D FS pocket centred at the Z -point, as pointed out previously [5,20].

To check whether the SC gap follows the same modulations as the Fermi momentum k_F , we performed high-resolution SC gap measurements at different k_z values. The results for the γ band are shown in fig. 2. We display in fig. 2(a) the intensity plot of a cut recorded at 0.9 K with $\hbar\nu = 30$ eV that crosses the \bar{M} -point, which has been symmetrized with respect to E_F following a common practice, to approximately remove the contribution of the Fermi-Dirac function at the k_F points in the SC state. A SC gap opening with a strong coherent peak and the bending back in the dispersion characterizing the SC state are clearly observed. Using this procedure, one can identify precisely the minimum gap location, which corresponds to k_F . The location of the k_F points on the γ FS where the SC gap has been measured using 30 eV photons is given by circles in fig. 2(b). The corresponding symmetrized EDCs, shown in fig. 2(c), indicate a nearly isotropic SC gap Δ , defined by half the distance between the two peaks, which averages to 8.2 meV. This value is consistent with our previous study on the same material using the $I\alpha$ line of a helium discharge lamp [4]. In fig. 2(d), we show additional symmetrized EDCs recorded with photon energies ranging from 18 eV to 32 eV, which covers the k_z range indicated in fig. 2(b). Our results indicate that the gap size associated with the γ band is quite k_z -insensitive.

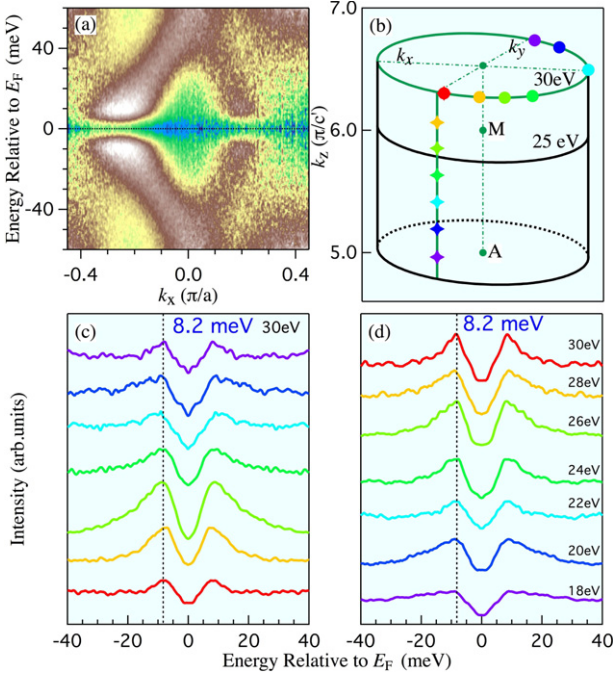


Fig. 2: (Colour on-line) (a) Symmetrized ARPES intensity plot of the γ band for $h\nu = 30$ eV. (b) Schematic 3D γ FS and k_F locations of the EDCs used for the SC gap measurements. (c) Symmetrized ARPES spectra in the SC state (0.9 K) measured with $h\nu = 30$ eV at various k_F points indicated by circles in (b). (d) Symmetrized EDCs at various k_F positions along the k_z axis indicated in (b) with diamonds. The colour of the EDCs in (c), (d) refers to the symbol of the k_F indicators in (b). Dashed lines are guides to the eye.

We now turn our attention to the 3D κ FS pocket, for which we performed similar measurements and analysis. The results are reported in fig. 3. In panel (a) we show the FS intensity map obtained at 30 eV around the Z-point ($k_z \sim \pi$). A series of symmetrized intensity plots along the cuts identified in fig. 3(a), is given in panels (b)–(f). These cuts illustrate that a SC gap opens everywhere along the $k_z = \pi$ section of the κ FS. The temperature evolution of the k_F EDCs given in panel (g) shows that the gap fills up above the SC transition ($T_c = 29$ K), confirming its SC nature. We note that this behaviour is reversible upon thermal cycle. The symmetrized EDCs corresponding to the k_F positions of the cuts # 1 to # 5 in fig. 3(b)–(f) are displayed in fig. 3(h). Although the precise determination of the SC gap size would allow larger anisotropy ($\leq 20\%$) than for the γ band, the SC gap of the κ band is also nodeless and quite isotropic in this particular k_z plane. The averaged SC gap value for $h\nu = 30$ eV is approximately 6.2 meV, which is smaller than that of the γ FS but still in the strong-coupling regime ($2\Delta/k_B T_c \sim 5$). To investigate possible SC gap modulation along the dispersive k_z direction, we tuned the photon energy between 20 eV and 30 eV. The corresponding symmetrized EDCs are displayed in fig. 3(i). Surprisingly, the SC gap

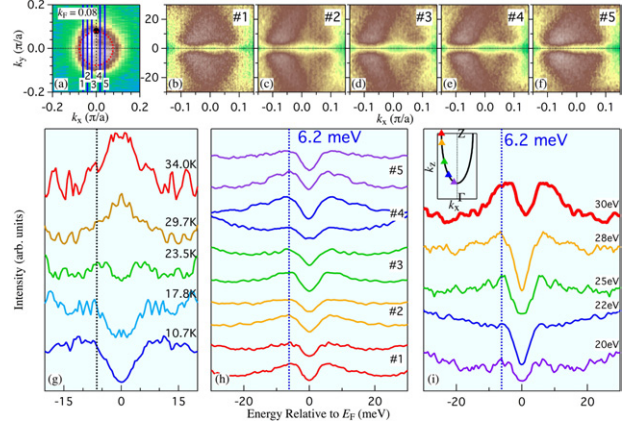


Fig. 3: (Colour on-line) (a) ARPES intensity map around $Z(0,0,\pi)$ with photon energy 30 eV. The red dashed line indicates the FS position with $k_F \sim 0.08\pi/a$. (b)–(f) Symmetrized ARPES intensity plots recorded in the SC state (0.9 K) along cuts # 1 to # 5 indicated by blue lines in (a). (g) Temperature dependence of symmetrized EDC spectra at k_F . The black dot in (a) shows the k_F location of the EDCs. (h), (i) Symmetrized EDCs in the SC state (0.9 K) measured at various k_F points along the κ FS in the $k_z = \pi$ plane, and along k_z , respectively. The k_F positions in (i) are indicated in the inset. Dashed lines are guides to the eye.

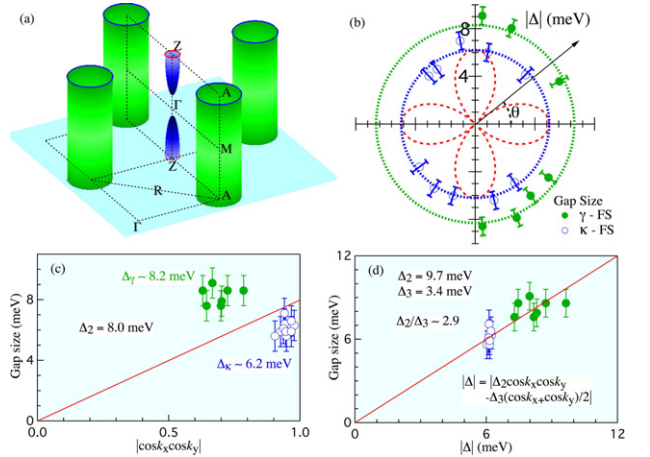


Fig. 4: (Colour on-line) (a) 3D representation of the FS of $\text{Tl}_{0.63}\text{K}_{0.37}\text{Fe}_{1.78}\text{Se}_2$. (b) Polar representation of the SC gap associated with the κ and γ FSs at 0.9 K and $h\nu = 30$ eV (near $k_z \sim \pi$). The red dashed line indicate a d -wave profile. (c), (d) SC gap values at 30 eV plotted as a function of $|\cos k_x \cos k_y|$ and $|\Delta_2 \cos k_x \cos k_y - \Delta_3 (\cos 2k_x + \cos 2k_y)/2|$, respectively.

size is robust against the strong modulations of the FS, indicating a full 3D SC gap with s -wave symmetry.

Our main results on the SC gap in $\text{Tl}_{0.63}\text{K}_{0.37}\text{Fe}_{1.78}\text{Se}_2$ are summarized in fig. 4. The FS topology illustrated in fig. 4(a), with the absence of hole FS [4–7,20], seems inconsistent with electron-hole quasi-nesting pairing mechanisms. The complete SC gap structure, which is directly shaped by the SC pairing mechanism, can narrow further the list of the pairing candidates. In fig. 4(b) we show the

polar representation of the SC gap measured for the κ and γ FSs. As mentioned above, these gaps are nodeless and isotropic within experimental uncertainties, and they show no obvious variation along k_z . While the isotropy of the SC gap around \bar{M} does not directly exclude a global $d_{x^2-y^2}$ -wave symmetry with nodes along the $k_x = \pm k_y$ directions, the one of the κ FS pocket elongated along the Γ - Z direction is a strong evidence against such pairing symmetry. On the contrary, it is rather consistent with bulk-sensitive nuclear magnetic resonance [22] and specific heat measurements [23] which suggest the absence of node in the SC gap structure. One could argue that an s -wave pairing on the 3D FS pocket at Z may coexist with a d -wave pairing on the large 2D FS around \bar{M} and that the different pairings are only weakly coupled. However, such an “hybrid” pairing scenario usually has different pairing strengths and different transition temperatures above which the SC gap closes. Our observation of the same temperature dependence on both FSs does not support this scenario.

An s -wave symmetry can be derived from various theoretical approaches. The conventional s_{\pm} symmetry with a sign reversal between Γ and M can be obtained from an effective J_1 - J_2 model [14–17,19,24] while the valence band Suhl-Kondo effect can lead to an s_{++} pairing symmetry, without any phase sign change [11]. Weak-coupling scenarios including orbital fluctuations [11] and charge fluctuations [25] may also lead to an s_{++} pairing symmetry, while a “bonding-antibonding” s_{\pm} symmetry with a sign reversal between two concentric M -centred FS pockets without any node in the whole k -space was proposed based on a spin fluctuations approach [9]. Even though our k -sensitive but phase-insensitive ARPES measurements do not allow us to identify directly which of the s -wave pairing symmetries is the correct one, the relative gap size on the various FSs may give some hints on the relevant pairing mechanism.

Recently, a careful ARPES study of the SC gap in the cousin $\text{FeTe}_{0.55}\text{Se}_{0.45}$ ferrochalcogenide superconductor reported nearly isotropic SC gaps with a larger gap at the M -point [26]. While the SC gap of most ferropnictide superconductors is roughly consistent with a $|\cos k_x \cos k_y|$ gap function [27–29] that can be derived from a J_1 - J_2 model [14], where J_1 and J_2 characterize the nearest- and next-nearest-neighbor magnetic exchange interaction couplings, the global SC gap structure in $\text{FeTe}_{0.55}\text{Se}_{0.45}$ rather follows a $|\Delta_2 \cos k_x \cos k_y - \Delta_3 (\cos 2k_x + \cos 2k_y)/2|$ function consistent with a non-negligible J_3 constant [15]. In order to check if either of these gap functions applies to $\text{Tl}_{0.63}\text{K}_{0.37}\text{Fe}_{1.78}\text{Se}_2$, we show in figs. 4(c) and (d) fits of our SC gap data to the J_1 - J_2 and J_1 - J_2 - J_3 gap functions, respectively. While the data are clearly inconsistent with the former model, the latter works reasonably well. From the fit to the $|\Delta_2 \cos k_x \cos k_y - \Delta_3 (\cos 2k_x + \cos 2k_y)/2|$ gap function, we obtain the global SC gap parameters $\Delta_2 = 9.7$ meV and $\Delta_3 = 3.4$ meV. Their ratio gives 2.9, which is not much different but smaller than the ~ 3.7 ratio obtained

in $\text{FeTe}_{0.55}\text{Se}_{0.45}$ [26], suggesting a stronger J_3 coupling constant. Within the J_1 - J_2 - J_3 model, an increase in the J_3 strength (or a decrease in the J_2/J_3 ratio) is consistent with the observation of a strong Se $4p_z$ orbital component for the κ band in $(\text{Tl}, \text{Rb})_y\text{Fe}_{2-x}\text{Se}_2$ [20], which favors the Se-bridged superexchange interaction that can enhance J_3 . However, we notice that the latter fit has a good degree of uncertainty, and more precise measurements are needed in order to make a definite claim.

In summary, we fully characterized the SC gap of $\text{Tl}_{0.63}\text{K}_{0.37}\text{Fe}_{1.78}\text{Se}_2$ over the whole BZ, including the small 3D electron pocket centred at Z . All gaps are nodeless and do not show significant momentum dependence, thus ruling out any d -wave pairing scenario in this system. Moreover, all SC gap data can be fit with a single-gap function derived from a strong-coupling approach.

We are grateful to J.-P. HU for useful discussions. This work is supported by the Chinese Academy of Sciences (grant No. 2010Y1JB6), the Ministry of Science and Technology of China (grants No. 2010CB923000, No. 2011CBA0010), and the Nature Science Foundation of China (grants No. 10974175, No. 11004232, and No. 11050110422). This work was supported by the Sino-Swiss Science and Technology Cooperation (project no. IZLCZ2 138954). This work was partly performed at the Swiss Light Source, Paul Scherrer Institut, Villigen, Switzerland, and at BESSY, Helmholtz Zentrum, Berlin, Germany.

REFERENCES

- [1] RICHARD P., SATO T., NAKAYAMA K., TAKAHASHI T. and DING H., *Rep. Prog. Phys.*, **74** (2011) 124512.
- [2] GUO JIANGANG, JIN SHIFENG, WANG GANG, WANG SHUNCHONG, ZHU KAIXING, ZHOU TINGTING, HE MENG and CHEN XIAOLONG, *Phys. Rev. B*, **82** (2010) 180520(R).
- [3] FANG M.-H., WANG H.-D., DONG C.-H., LI Z.-J., FENG C.-M., CHEN J. and YUAN H. Q., *EPL*, **94** (2011) 27009.
- [4] WANG X.-P., QIAN T., RICHARD P., ZHANG P., DONG J., WANG H.-D., DONG C.-H., FANG M.-H. and DING H., *EPL*, **93** (2011) 57001.
- [5] ZHANG Y., YANG L. X., XU M., YE Z. R., CHEN F., HE C., JIANG J., XIE B. P., YING J. J., WANG X. F., CHEN X. H., HU J. P. and FENG D. L., *Nat. Mater.*, **10** (2011) 273.
- [6] MOU D., LIU S., JIA X., HE J., PENG Y., ZHAO L., YU L., LIU G., HE S., DONG X., ZHANG J., WANG H., DONG C., FANG M., WANG X., PENG Q., WANG Z., ZHANG S., YANG F., XU Z., CHEN C. and ZHOU X. J., *Phys. Rev. Lett.*, **106** (2011) 107001.
- [7] QIAN T., WANG X.-P., JIN W.-C., ZHANG P., RICHARD P., XU G., DAI X., FANG Z., GUO J.-G., CHEN X.-L. and DING H., *Phys. Rev. Lett.*, **106** (2011) 187001.
- [8] WANG F., YANG F., GAO M., LU Z.-Y., XIANG T. and LEE D.-H., *EPL*, **93** (2011) 57003.
- [9] MAZIN I. I., *Phys. Rev. B*, **84** (2011) 024529.

- [10] MAIER T. A., GRASER S., HIRSCHFELD P. J. and SCALAPINO D. J., *Phys. Rev. B*, **83** (2011) 100515(R).
- [11] SAITO T., ONARI S. and KONTANI H., *Phys. Rev. B*, **83** (2011) 140512(R).
- [12] DAS T. and BALATSKY A. V., *Phys. Rev. B*, **84** (2011) 014521.
- [13] ZHOU T. and WANG Z. D., arXiv:1202.1607 (2012).
- [14] SEO K., BERNEVIG B. A. and HU J. P., *Phys. Rev. Lett.*, **101** (2008) 206404.
- [15] FANG C., WU Y.-L., THOMALE R., BERNEVIG B. A. and HU J.-P., *Phys. Rev. X*, **1** (2011) 011009.
- [16] HU JIANGPING and DING HONG, *Sci. Rep.*, **2** (2012) 381.
- [17] YU R., GOSWAMI P., SI Q.-M., NIKOLIC P. and ZHU J.-X., arXiv:1103.3259 (2011).
- [18] ZHOU Y., XU D.-H., ZHANG F.-C. and CHEN W.-Q., *EPL*, **95** (2011) 17003.
- [19] HU J.-P. and HAO N.-N., *Phys. Rev. X*, **2** (2012) 021009.
- [20] LIU Z.-H., RICHARD P., XU N., XU G., LI Y., FANG X.-C., JIA L.-L., CHEN G.-F., WANG D.-M., HE J.-B., QIAN T., HU J.-P., DING H. and WANG S.-C., *Phys. Rev. Lett.*, **109** (2012) 037003.
- [21] HÜFNER S., *Photoelectron Spectroscopy* (Springer-Verlag, Berlin) 2011.
- [22] YU W. Q., MA L., HE J. B., WANG D. M., XIA T.-L., CHEN G. F. and BAO W., *Phys. Rev. Lett.*, **106** (2011) 197001.
- [23] ZENG B., SHEN B., CHEN G. F., HE J. B., WANG D. M., LI C. H. and WEN H. H., *Phys. Rev. B*, **83** (2011) 144511.
- [24] LU X., FANG C., TSAI W.-F., JIANG Y.-J. and HU J. P., *Phys. Rev. B*, **85** (2012) 054505.
- [25] ZHOU S., KOTLIAR G. and WANG Z., *Phys. Rev. B*, **84** (2011) 140505(R).
- [26] MIAO H., RICHARD P., TANAKA Y., NAKAYAMA K., QIAN T., UMEZAWA K., SATO T., XU Y.-M., SHI Y.-B., XU N., WANG X.-P., ZHANG P., YANG H.-B., XU Z.-J., WEN J. S., GU G.-D., DAI X., HU J.-P., TAKAHASHI T. and DING H., *Phys. Rev. B*, **85** (2012) 094506.
- [27] NAKAYAMA K., SATO T., RICHARD P., XU Y.-M., SEKIBA Y., SOUMA S., CHEN G. F., LUO J. L., WANG N. L., DING H. and TAKAHASHI T., *EPL*, **85** (2009) 67002.
- [28] NAKAYAMA K., SATO T., RICHARD P., XU Y.-M., KAWAHARA T., UMEZAWA K., QIAN T., NEUPANE M., CHEN G. F., DING H. and TAKAHASHI T., *Phys. Rev. B*, **83** (2011) 020501(R).
- [29] LIU Z.-H., RICHARD P., NAKAYAMA K., CHEN G.-F., DONG S., HE J.-B., WANG D.-M., XIA T.-L., UMEZAWA K., KAWAHARA T., SOUMA S., SATO T., TAKAHASHI T., QIAN T., YAObOHUANG, NAN XU, YINGBO SHI, DING H. and WANG S.-C., *Phys. Rev. B*, **84** (2011) 064519.